

SUSY QCD corrections to electroweak gauge boson production with an associated jet at the LHC

Ryan Gavin

*Phenomenology Institute, Department of Physics, University of Wisconsin-Madison,
1150 University Avenue, Madison, Wisconsin 53706, USA*

and

Paul Scherrer Institut, CH-5232 Villigen PSI, Switzerland

Email: ryan.gavin@psi.ch

Maïke K. Trenkel

*Phenomenology Institute, Department of Physics, University of Wisconsin-Madison,
1150 University Avenue, Madison, Wisconsin 53706, USA*

Email: trenkel@hep.wisc.edu

ABSTRACT: We study the stability of the neutral- and charged-current Drell–Yan process in association with a jet as a standard candle at the LHC under the inclusion of $\mathcal{O}(\alpha_s)$ supersymmetric QCD (SQCD) corrections within the MSSM. We include the decay of the electroweak gauge boson into dileptons, i.e. we consider the production of charged lepton–anti-lepton or lepton-neutrino final states with one hard jet. We find that the SQCD corrections are negligible for the integrated cross section. Only at high lepton transverse momentum can they induce effects of the percent level.

KEYWORDS: [Supersymmetry Phenomenology](#), [NLO Computations](#), [Hadronic Colliders](#).

Contents

1. Introduction	1
2. Details of the calculation	3
2.1 Leading order processes	3
2.2 NLO SQCD corrections	4
3. Numerical results	6
3.1 Input parameters	7
3.2 Z/γ^* +jet integrated cross section results	8
3.3 Z/γ^* +jet kinematic distributions	9
3.4 W +jet integrated cross section results	10
3.5 W +jet kinematic distributions	12
4. Conclusions	14
A. Counterterms and renormalization constants	15

1. Introduction

Electroweak gauge boson production with subsequent leptonic decays plays a crucial role in the physics studies performed at hadron colliders. With large cross sections and a clear collider signature, the Drell–Yan processes have become a standard candle at the LHC and many precise measurements are currently being performed [1–4]. Their study can be used to help calibrate detectors and place constraints on parton distribution functions (PDFs), see e. g. [5–7]. It has also been proposed that measured electroweak boson production cross sections can be used as a luminosity monitor [8]. Drell–Yan processes also constitute an important source of background for searches for new physics, such as Z' and W' boson production and other high mass dilepton resonances [9–12].

Given the large amount of data that the LHC will deliver, measurement errors will eventually be dominated by systematics rather than statistics, see e. g. [13]. Consequently, electroweak boson production needs to be known to high precision. Much effort has been made in this area. Indeed, it was the first hadronic scattering process to be computed at next-to-next-to-leading (NNLO) in QCD [14, 15]. Now also the differential cross sections for Drell–Yan processes are known through NNLO in QCD [16–21], and the NLO QCD corrections have been matched to parton showers [22–25]. Electroweak corrections have been known for sometime [26–29], and continue to be refined [24, 30–34]. Attempts to approximate $\text{QCD} \times \text{EW}$ corrections to Drell–Yan have also appeared in the literature [34, 35] and very recently the mixed $\text{QCD} \times \text{EW}$ two-loop virtual corrections have been calculated [36].

At hadron colliders, the high center-of-mass energy (c.m.) typically leads to production of electroweak gauge bosons in association with QCD radiation. Here, we focus on Drell–Yan processes with one additional, hard jet. The intermediate gauge boson then recoils against the jet and can be strongly boosted. If the jet has large transverse momentum, the leptons originating from the gauge boson decay are produced at high transverse momentum as well and provide a source for either high-energy dilepton pairs of opposite charge (Z/γ^* +jet production) or high missing transverse energy in combination with a charged lepton (W +jet production). Theoretical predictions for the Drell–Yan+jet cross section include NLO QCD corrections [37–39] and parton shower matching [22], as well as in the electroweak sector the NLO corrections in the on-shell approximation [40–44] and the full NLO calculation, including photonic corrections and including the leptonic decay of the gauge boson [45,46]. Also for Drell–Yan cross sections with higher jet multiplicities, the NLO QCD corrections are now available [39,47–50].

Often, precision measurements of Standard Model (SM) processes are used to constrain new physics, not by direct detection, but by their influence through quantum fluctuations. One may ask the question how radiative corrections from physics beyond the Standard Model (BSM) would effect such well-known processes. To allow for precision tests of the SM and its perturbative expansions, it is crucial to know if there were large BSM corrections since otherwise information about the underlying physics cannot reliably be extracted from the data. An interesting paradigm for physics beyond the SM is supersymmetry (SUSY). Many collider studies have been performed to examine the phenomenology of SUSY production at hadron colliders, and the possibility of their detection. The investigation of new physics contributions to SM processes via higher-order corrections is a logical next step. Only in recent years, Drell–Yan processes have been studied within the framework of the minimal supersymmetric Standard Model (MSSM). The NLO supersymmetric QCD (SQCD) and electroweak corrections within the MSSM to the charged- and neutral-current Drell–Yan processes with no final state parton were calculated in [30,31] and the NLO electroweak corrections for the on-shell W +jet production process within MSSM have been computed in [51]. The impact of SUSY corrections has been found to be small.

In this work, we further complete the one-loop picture and calculate the NLO SQCD corrections within the MSSM to Drell–Yan processes in association with a hard jet in the final state. We consider both Z/γ^* +jet and W +jet production at the LHC, including the leptonic decay of the gauge bosons, and take all off-shell effects due to the finite widths of the Z and W boson and all contributions of an intermediate photon into account. Our aim is to show the stability of Drell–Yan+jet processes under the inclusion of SQCD corrections within the MSSM.

This paper is organized as follows. The setup of the calculation is detailed in section 2. The computation of the SQCD corrections to the neutral- and charged-current Drell–Yan processes proceed in close analogy and are discussed in parallel. In section 3 we present the numerical results for both Z/γ^* +jet and W +jet production at the LHC. We summarize our findings in section 4. Details on the renormalization procedure are given in appendix A.

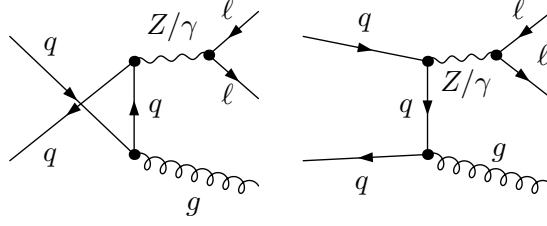


Figure 1: Feynman diagrams for the quark–anti-quark initial state process, Eq. (2.1).

2. Details of the calculation

In this section we describe the technical setup of our calculation of SQCD corrections for the neutral- and charged-current Drell–Yan process with an associated hard jet. We always include the decay of the gauge bosons into leptons and take all off-shell effects due to the finite width of the Z or W boson into account. We first address the leading order (LO) processes in section 2.1 and then discuss the NLO calculation in section 2.2. In view of SQCD corrections, the computations for $Z/\gamma^* + \text{jet}$ and $W + \text{jet}$ production are very similar and proceed in close analogy.

2.1 Leading order processes

At the LHC, the Drell–Yan process in association with a hard jet is initiated by three different partonic processes at LO. Including the leptonic decay of the intermediate electroweak gauge boson, they are in the case of the neutral-current Drell–Yan process,

$$q \bar{q} \rightarrow Z/\gamma^* g \rightarrow \ell^- \ell^+ g, \quad (2.1)$$

$$g q \rightarrow Z/\gamma^* q \rightarrow \ell^- \ell^+ q, \quad (2.2)$$

$$g \bar{q} \rightarrow Z/\gamma^* \bar{q} \rightarrow \ell^- \ell^+ \bar{q}, \quad (2.3)$$

and for the charged-current Drell–Yan process,

$$q \bar{q}' \rightarrow W g \rightarrow \ell \nu_\ell g, \quad (2.4)$$

$$g q \rightarrow W q' \rightarrow \ell \nu_\ell q', \quad (2.5)$$

$$g \bar{q} \rightarrow W \bar{q}' \rightarrow \ell \nu_\ell \bar{q}'. \quad (2.6)$$

For W^+ production, a positively charged lepton is produced together with an anti-neutrino ($\ell^+ \bar{\nu}_\ell$), for W^- production it is a negatively charged lepton and a neutrino ($\ell^- \nu_\ell$).

The tree-level Feynman diagrams for the process Eq. (2.1) can be found in Figure 1, those for $W + \text{jet}$ production follow analogously by replacing the Zqq ($Z\ell\ell$) vertex with a Wqq' ($W\ell\nu_\ell$) vertex. Diagrams for the (anti-)quark–gluon processes are obtained by crossing the gluon with an initial-state (anti-)quark.

The quarks considered are $q, q' = u, c, d, s$ with q and q' being quarks of opposite isospin. The quarks are treated as massless throughout the calculation. The $Z/\gamma^* + \text{jet}$ LO cross section is quark generation independent, aside from the appropriate PDF inclusion and convolution. The only up- and down-type quark dependence comes from the vector

and axial couplings in the $Zq\bar{q}$ vertex. The W +jet cross sections do depend on the quark flavor due to the quark mixing parameterized by the CKM matrix. However, the CKM quark mixing factorizes from the tree-level matrix elements and, for the inclusive cross section, there needs only one squared amplitude to be calculated for each of three partonic channels, weighted by the sum of squares of the respective absolute value elements of the CKM matrix, as well as the corresponding PDFs.

Throughout the calculation, we exclude bottom-quark initiated processes due to their PDF-suppressed small contribution to the cross section and we neglect the mixing between first and third generation quarks. A fixed width is included in the propagator of the intermediate Z or W boson, giving the expected Breit-Wigner resonance.

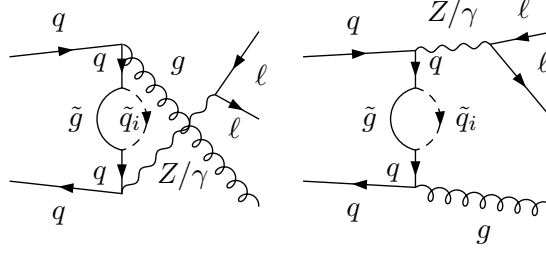
Already at LO, there exists the possibility that the parton in the final state may become soft or collinear to the gluon or quark that it couples to. If this occurs, the cross section becomes infinite. Divergences of this type are regulated by requiring the jet to be hard. This is achieved by applying a minimum transverse-momentum (p_T) cut on the jet. Also we treat the leptons as massless throughout the calculation and require a minimum lepton p_T as well as a minimum lepton-pair invariant mass, $M_{\ell\ell}$, in case of Z/γ^* +jet production.

2.2 NLO SQCD corrections

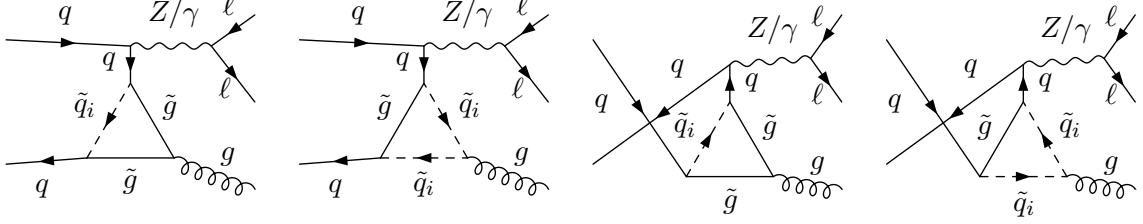
We calculate the one-loop SQCD corrections to the partonic processes in Eqs. 2.1-2.3 and Eqs. 2.4-2.6, which are purely virtual. The SUSY particles charged under $SU(3)_C$ are the squarks, \tilde{q}_i , and gluinos, \tilde{g} , the superpartners of the SM chiral quarks and gluons, respectively. In the SM, left- and right-handed quarks transform differently under $SU(2)_L$. Consequently, under supersymmetric transformations, there are separate superpartners, \tilde{q}_L , \tilde{q}_R , for quarks of different handedness, q_L , q_R . After electroweak symmetry breaking (EWSB), left- and right-handed squark eigenstates mix to form squark mass eigenstates, \tilde{q}_1 , \tilde{q}_2 . Squark mixing, however, is proportional to the mass of their SM quark partner. In this calculation, only squarks of the same flavor as the initial state quarks are present. Since the masses of the quarks considered (u , d , c , s) are small, we can neglect any left-right mixing between squark eigenstates, and the two gauge eigenstates of a given flavor q are also mass eigenstates that we denote by \tilde{q}_i , $i = L, R$.

In the calculation of Z/γ^* +jet production, the relevant interactions between SM and SUSY particles are the $\gamma\tilde{q}_i\tilde{q}_j$, $Z\tilde{q}_i\tilde{q}_j$, $g\tilde{q}_i\tilde{q}_i$, $g\tilde{g}\tilde{g}$, and $q\tilde{q}_i\tilde{g}$ vertices. Although there are diagrams with the $\gamma g\tilde{q}_i\tilde{q}_j$ or $Zg\tilde{q}_i\tilde{q}_j$ vertex, their contribution to the virtual corrections is zero, and they have not been explicitly included in this manuscript. There are 44 diagrams per partonic channel that give non-zero contributions to the differential cross section (22 for Z boson and photon mediation each). They divide into self-energy insertions, gluon- and Z/γ^* -vertex corrections, and box contributions and are organized in Figure 2. In each diagram, the two squark eigenstates \tilde{q}_i of the same quark flavor q as the initial state can run in the loop. The Feynman diagrams for W +jet production can easily be inferred from Figure 2 by again replacing the Zqq ($Z\ell\ell$) vertex with a Wqq' ($W\ell\nu_\ell$) vertex and by replacing the $Z\tilde{q}_i\tilde{q}_i$ by $W\tilde{q}_i\tilde{q}'_i$ vertices. Of course the W boson couples to left-handed particles only, and only the left-handed components of the squark eigenstates contribute (i.e. $\tilde{q}_i = \tilde{q}_L$ in case of no left-right mixing).

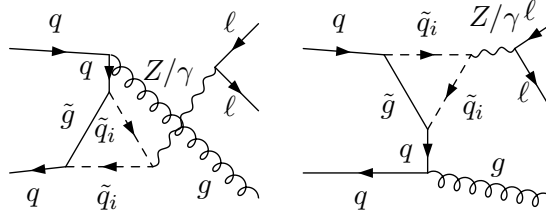
(a) Self-energy insertions:



(b) Gluon-vertex corrections:



(c) Z/γ^* -vertex corrections:



(d) Box contributions:

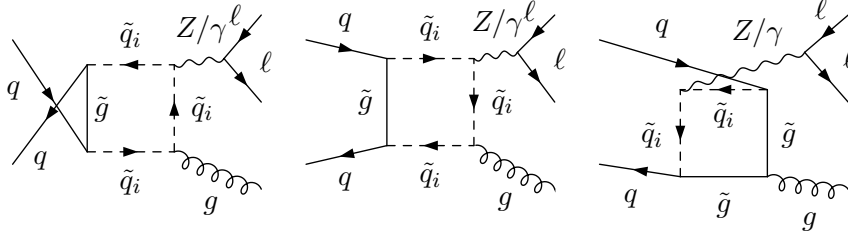


Figure 2: Feynman diagrams for the self-energy, gluon- and Z/γ^* -vertex, and box contributions to the partonic process $q\bar{q} \rightarrow \ell^+\ell^-g$, mediated by Z/γ^* exchange, at SQCD NLO.

Due to only massive particles propagating in the loop, the virtual corrections are completely infrared (IR) safe. Therefore, there are no real emission processes to be considered to cancel singularities. However, as noted above, we require a hard jet in the final state. This statement implies a minimum cut has been placed on the transverse momentum of the jet to avoid IR divergences that would otherwise appear at LO.

Ultraviolet (UV) divergences arise from the self-energy insertions and the gluon and Z/γ^* or W vertex corrections, while the box diagrams are IR and UV finite. Dimensional

regularization is used to regulate the UV divergences, where the number of dimensions is $d = 4 - 2\epsilon$ and the singularities then take the form of $1/\epsilon$ poles. In order to remove the UV divergences one has to include the proper counterterms for SQCD one-loop renormalization. Our renormalization procedure closely follows ref. [52]. We impose on-shell conditions to fix the renormalization constants in the quark sector and use the $\overline{\text{MS}}$ scheme, modified to decouple the heavy SUSY particles [53, 54], for the renormalization of the strong coupling constant and the gluon field. The explicit expressions in terms of the renormalization constants can be found in appendix A.

We set up the calculation in the conventional diagrammatic approach. As an important cross-check on the numerical results, two completely independent computations were performed using different techniques. The first calculation is based on the framework of FeynArts 3.6 [55], FormCalc 7.0, and LoopTools 2.6 [56]. In the second calculation, Feynman diagrams are generated with QGRAF [57]. Algebraic manipulation is performed with an in-house software comprised of Maple and Form [58]. Then AIR [59] is used for the reduction of tensor loop integrals to scalar ones. The numerical integration is performed using Vegas of the Cuba 1.7 [60] library, as well as the scalar loop integral library QCDLoop [61].

The Zqq , Wqq' , $Z\tilde{q}_i\tilde{q}_j$, $W\tilde{q}_i\tilde{q}'_j$, and $q\tilde{q}\tilde{g}$ vertices contain axial pieces. Special attention should be paid to the treatment of γ^5 when working in d dimensions. In the first calculation the naive anticommuting scheme [56, 62] was used. Here, it is assumed that $\{\gamma^5, \gamma^\mu\} = 0$ as in four space-time dimensions and that the four-dimensional, non-zero trace,

$$\text{Tr}[\gamma^\mu\gamma^\nu\gamma^\rho\gamma^\sigma\gamma^5] = -4i\epsilon^{\mu\nu\rho\sigma}, \quad (2.7)$$

remains. This FormCalc-based approach has been justified in [63]. In the second calculation, the treatment of γ^5 as described in [64] is used, where

$$\gamma^5 = \frac{i}{4!}\epsilon_{\mu\nu\rho\sigma}\gamma^\mu\gamma^\nu\gamma^\rho\gamma^\sigma. \quad (2.8)$$

Both approaches have been shown to give consistent results in our NLO calculation.

3. Numerical results

In this section we investigate the numerical influence of the SQCD one-loop corrections to both the neutral- and charged current Drell–Yan process with an associated hard jet. We examine these processes at the LHC with a c.m. energy of 7 TeV, unless noted otherwise. We list the relevant input parameters in section 3.1. The integrated cross section results and differential distributions for the $Z/\gamma^* + \text{jet}$ process are given in sections 3.2 and 3.3, respectively. The results for $W + \text{jet}$ production are discussed in sections 3.4 and 3.5.

3.1 Input parameters

The SM input parameters are chosen in accordance with [65],

$$\begin{aligned}
M_Z &= 91.1876 \text{ GeV}, & M_W &= 80.339 \text{ GeV}, \\
\Gamma_Z &= 2.4952 \text{ GeV}, & \Gamma_W &= 2.085 \text{ GeV}, \\
\cos \theta_W &= M_W/M_Z, & \alpha^{-1} &= \alpha(M_Z)^{-1} = 128.91, \\
|V_{ud}| &= 0.97428, & |V_{us}| &= 0.2253, & |V_{cd}| &= 0.2252, & |V_{cs}| &= 0.97345.
\end{aligned} \tag{3.1}$$

Quarks and leptons are considered massless and we do not further specify the flavor of the leptons in the final state as the SQCD corrections do not depend on the lepton flavor. Factorization and renormalization scales are fixed and identified with the vector boson mass, $\mu_F = \mu_R = M_{Z,W}$. We use the central MSTW 2008 NLO (68% CL) PDF set [66] in its LHAPDF implementation [67], with the strong coupling $\alpha_s(\mu_R)$ they provide, yielding

$$\alpha_s(M_Z) = 0.12018, \quad \alpha_s(M_W) = 0.12257. \tag{3.2}$$

We require a set of basic kinematic cuts to be satisfied. As previously mentioned, a minimum p_T of the final state parton is required to render the cross section finite. We also demand the two final-state leptons to have a minimum transverse momentum. Furthermore we require the leptons and the jet to be produced in the central region of the detector and apply a cut on their rapidities. For the Z/γ^* +jet process we also require a minimum lepton-pair invariant mass, $M_{\ell\ell}$. We choose the following numerical values,

$$\begin{aligned}
Z/\gamma^* + \text{jet} : \quad & p_{T,\text{jet}} > 25 \text{ GeV}, & |y_{\text{jet}}| < 2.5, \\
& p_{T,\ell^\pm} > 25 \text{ GeV}, & |y_{\ell^\pm}| < 2.5, & M_{\ell\ell} > 50 \text{ GeV}. \\
W + \text{jet} : \quad & p_{T,\text{jet}} > 25 \text{ GeV}, & |y_{\text{jet}}| < 2.5, \\
& p_{T,\ell}, \not{p}_T > 25 \text{ GeV}, & |y_\ell| < 2.5.
\end{aligned} \tag{3.3}$$

However, only the integrated cross sections depend strongly on the specific cuts chosen, while we have found that the relative importance of the SQCD corrections does not vary much when the cuts are tightened or loosened.

The only SUSY particles that appear in the loops are squarks and the gluino. The SQCD corrections are flavor- and chirality-blind and no other SUSY parameters than the squark and gluino masses enter the calculation. For simplicity we neglect the squark left-right mixing, set all squark masses equal and use a common squark mass, $m_{\tilde{q}}$, and the gluino mass, $m_{\tilde{g}}$, as direct input. There is no need to define a complete set of SUSY input parameters and we do not consider commonly used benchmark scenarios (as e. g. SPS1a') here. As we will see below, this approach is sufficient for the purpose of our study to show the stability of Drell–Yan+jet under the inclusion of SQCD corrections. We use the following values for our numerical studies, if not otherwise noted,

$$m_{\tilde{q}} = 600 \text{ GeV}, \quad m_{\tilde{g}} = 500 \text{ GeV}. \tag{3.4}$$

These sparticle masses are already at the lower limit of the mass region that is currently investigated by LHC experiments, see e. g. [68,69], and allow for a conservative estimate of the typical size of SQCD corrections to Drell–Yan+jet processes.

$Z/\gamma^* + \text{jet}$ production	partonic channel	LO cross section	SQCD contributions	δ
$\sqrt{s} = 7 \text{ TeV}$	$q\bar{q}$	16.55 pb	0.987 fb	0.0059 %
	$gq + g\bar{q}$	37.73 pb	2.520 fb	0.0066 %
	incl.	54.27 pb	3.507 fb	0.0065 %
$\sqrt{s} = 14 \text{ TeV}$	$q\bar{q}$	31.70 pb	1.947 fb	0.0061 %
	$gq + g\bar{q}$	91.38 pb	6.798 fb	0.0074 %
	incl.	123.1 pb	8.746 fb	0.0071 %

Table 1: Numerical results for integrated cross sections for the neutral-current Drell–Yan process mediated by a Z boson or virtual photon γ^* in association with a hard jet at the LHC, with $\sqrt{s} = 7 \text{ TeV}$ and $\sqrt{s} = 14 \text{ TeV}$. Shown are the leading order results in picobarn (pb), the SQCD contributions in femtobarn (fb) and the relative corrections δ for the partonic subchannels and the inclusive result (incl.). Light quarks are implicitly summed over in the initial state, $q = u, d, c, s$. We consider $m_{\tilde{q}} = 600 \text{ GeV}$, $m_{\tilde{g}} = 500 \text{ GeV}$ and the cuts listed in Eq. (3.3) have been applied. Factorization and renormalization scale are set to $\mu = M_Z$ (with MSTW 2008 NLO) .

3.2 $Z/\gamma^* + \text{jet}$ integrated cross section results

Here we present the integrated cross section for charged dilepton production with a hard jet at the LHC. Table 1 shows the LO cross sections and SQCD contributions for the $q\bar{q}$ and gluon-initiated partonic processes, at a proton-proton c.m. energy of $\sqrt{s} = 7 \text{ TeV}$ and $\sqrt{s} = 14 \text{ TeV}$.

The prominent production modes at the LHC are the gluon-induced initial states, enhanced by the large gluon densities at small parton momentum fractions. With the kinematic constraints in Eq. (3.3), the total integrated cross section is 54.27 pb at 7 TeV and 123.1 pb at 14 TeV ($q = u, d, c, s$). The SQCD corrections, for squark and gluino masses of 600 and 500 GeV, respectively, account for an increase of 0.006% – 0.007% in the inclusive integrated cross section as well as per partonic channel. The c.m. energy at the LHC has little effect on the size of the corrections. Only the LO cross section strongly depends on the energy. When going from 7 TeV to 14 TeV, the gluon-quark channels become even more important and we find that at LO they contribute 74%. However, the SQCD effects on the integrated cross section remain basically unchanged and small in absolute value.

To further study the effects of SQCD corrections on the integrated cross section of $Z/\gamma^* + \text{jet}$ production, we show in Figure 3 the relative corrections as a function of the common squark mass $m_{\tilde{q}}$, for different values of the gluino mass. As one would expect, the impact of the SQCD corrections increases as the SUSY particle masses decrease. However, even for very light squarks and gluinos of only 100 GeV the relative corrections are still significantly below the 1% level. Figure 3 shows that the $Z/\gamma^* + \text{jet}$ integrated cross section is stable under SQCD corrections, over a broad range of low-mass squarks and gluinos. For TeV-range SUSY particles the SQCD corrections are completely negligible. This is

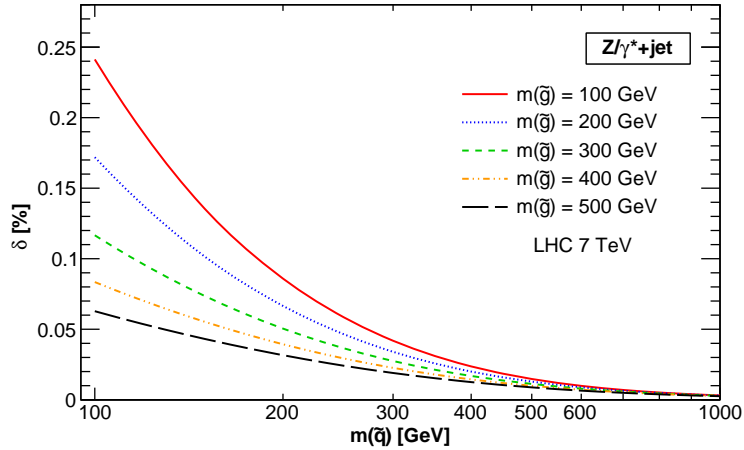


Figure 3: Relative SQCD corrections of the integrated cross section, $\delta = (\sigma_{NLO} - \sigma_{LO})/\sigma_{LO}$, for charged lepton-pair production mediated by a Z boson or virtual photon in association with a hard jet at the LHC, with $\sqrt{s} = 7$ TeV, as a function of a common squark mass, $m_{\tilde{q}}$, for different gluino masses, $m_{\tilde{g}}$. The cuts listed in Eq. (3.3) have been applied.

comforting in the sense that if $Z/\gamma^* + \text{jet}$ is used as a normalization process, no SUSY BSM physics should be masked in this normalization. In terms of our calculation, this stability also justifies our neglecting of squark left-right mixing, and use of a degenerate squark mass scheme.

3.3 $Z/\gamma^* + \text{jet}$ kinematic distributions

We have seen above that the SQCD contributions to the integrated cross section are subtle. However, the corrections can be more pronounced in the differential distributions of kinematic variables. We consider the LO and NLO differential cross sections, and define the relative corrections δ , $\delta = \frac{\mathcal{O}_{NLO} - \mathcal{O}_{LO}}{\mathcal{O}_{LO}}$, for a given observable \mathcal{O} , where \mathcal{O}_{NLO} is the sum of the LO contributions and the SQCD contributions. We present distributions in the lepton-pair invariant mass, $M_{\ell\ell}$, the lepton transverse momentum and rapidity, $p_{T,\ell}$ and y_ℓ , and the jet transverse momentum and rapidity, $p_{T,\text{jet}}$ and y_{jet} . All distributions shown have been subject to the kinematic constraints given in Eq. (3.3).

In Figure 4, distributions in the lepton-pair invariant mass $M_{\ell\ell}$ are displayed. We find that the SQCD corrections hardly affect the shape of the LO distribution and are below the 1% level for $M_{\ell\ell} < 1$ TeV (left panels). In the vicinity of the Z boson resonance, shown in the upper right panel, they are completely negligible and do not distort the SM result. For larger values of $M_{\ell\ell}$ (lower right panel) the relative corrections can reach several percent, until a SUSY mass threshold is reached and then the relative corrections begin to fall.

The lepton differential distributions in transverse momentum, $p_{T,\ell}$, and rapidity, y_ℓ , are given in Figure 5. In the low- and intermediate- p_T range, the SQCD contributions to the $p_{T,\ell}$ distribution are positive but small, increasing only to a maximum of about 1% at around the threshold of the average particle mass. In the high- p_T region, the relative corrections become non-negligible, on the order of a few negative percent. Concerning the

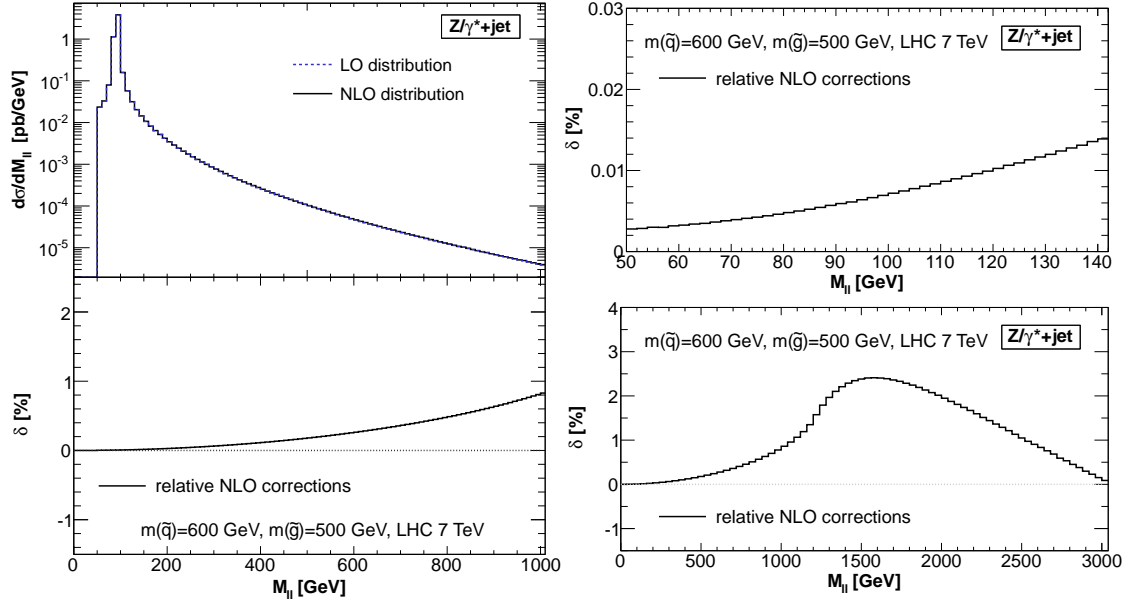


Figure 4: Differential distributions for the neutral-current Drell–Yan process in association with a hard jet at the LHC. NLO SQCD corrections are calculated for $m_{\tilde{q}} = 600$ GeV and $m_{\tilde{g}} = 500$ GeV and the cuts given in Eq. (3.3) have been placed. Shown are the absolute differential distributions for the LO and NLO processes (top left) and the relative difference between NLO and LO distributions (bottom left) with respect to lepton-pair invariant mass $M_{\ell\ell}$. In the right panels, the relative corrections around the Z boson resonance and in the high- $M_{\ell\ell}$ region are shown, respectively.

lepton rapidity, Figure 5 (right), we find that the relative corrections are nonzero but far below 1% and thus do not have any impact on the shape of the SM-only distribution. It is important to observe the discrepancies between the lepton and anti-lepton distributions in Figure 5. These differences occur already at the LO process and are a result of the Z boson’s axial coupling to fermions. Setting the axial coupling to zero would render the lepton and antilepton curves identical.

The jet distributions, Figure 6, exhibit the same behavior as the lepton distributions. We see the threshold effect around $(m_{\tilde{q}} + m_{\tilde{g}})/2$ is even more pronounced and the relative corrections in the high- $p_{T,\text{jet}}$ region ($p_T > 1.5$ TeV) contribute with roughly negative 4–5%, Figure 6 (left), while there are vanishing corrections to the jet rapidity, Figure 6 (right).

We also investigated differential distributions for lighter SUSY particles. We found a very similar picture as described above, with the SUSY threshold shifted accordingly, and abstain from showing the plots here. For $m_{\tilde{q}} = 400$ GeV and $m_{\tilde{g}} = 350$ GeV, the SQCD corrections become only slightly more important, and reach the 1–2% level at the sparticle thresholds and the –5% level for $p_T \approx 1500$ GeV.

3.4 W +jet integrated cross section results

In Table 2 we show the results for the integrated cross section for lepton-neutrino production with a hard jet, mediated by a W boson, at the LHC. The LO cross sections and SQCD contributions for the $q\bar{q}'$ and gluon-initiated partonic processes are given, at a proton-proton

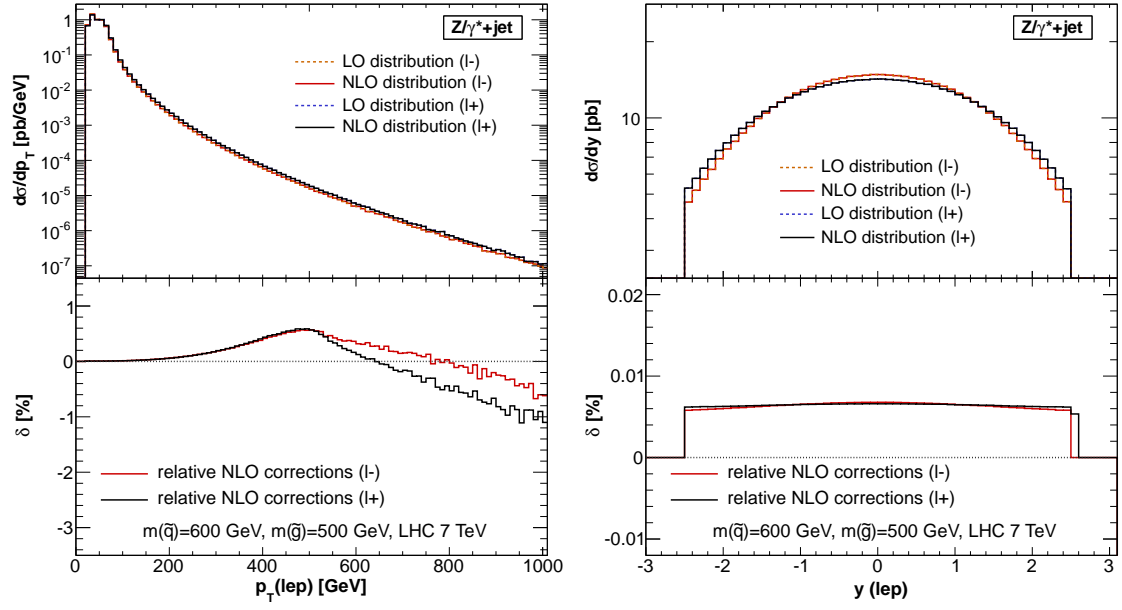


Figure 5: Lepton transverse momentum, $p_{T,\ell}$, (a) and lepton rapidity, y_ℓ , (b) distributions for the $Z/\gamma^*+\text{jet}$ process at the LHC with $\sqrt{s} = 7$ TeV. The black line represents the lepton while the red line represents the antilepton. NLO SQCD corrections are calculated for $m_{\bar{q}} = 600$ GeV and $m_{\bar{g}} = 500$ GeV and the cuts given in Eq. (3.3) have been placed.

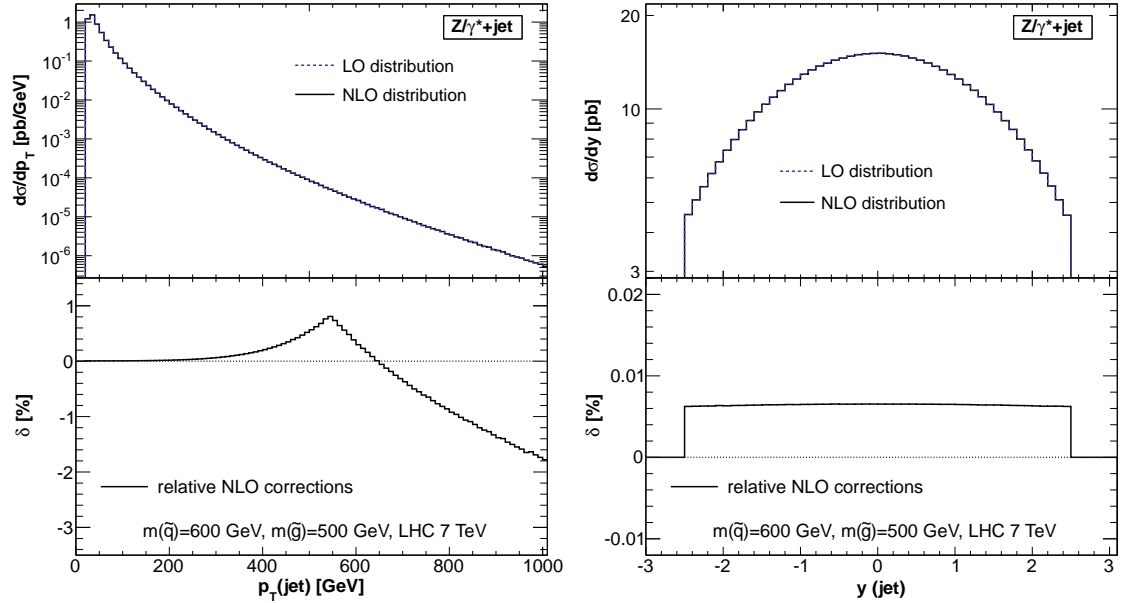


Figure 6: Jet transverse momentum, $p_{T,\text{jet}}$, (a) and jet rapidity, y_{jet} , (b) distributions for the $Z/\gamma^*+\text{jet}$ process at the LHC with $\sqrt{s} = 7$ TeV. NLO SQCD corrections are calculated for $m_{\bar{q}} = 600$ GeV and $m_{\bar{g}} = 500$ GeV and the cuts given in Eq. (3.3) have been placed.

W +jet production	partonic channel	LO cross section	SQCD contributions	δ
$\sqrt{s} = 7 \text{ TeV}$	$q\bar{q}'$	129.7 pb	5.746 fb	0.0044 %
	$gq + g\bar{q}$	342.1 pb	18.23 fb	0.0053 %
	incl.	471.9 pb	23.98 fb	0.0051 %
$\sqrt{s} = 14 \text{ TeV}$	$q\bar{q}'$	245.3 pb	10.81 fb	0.0044 %
	$gq + g\bar{q}$	810.9 pb	48.52 fb	0.0060 %
	incl.	1056 pb	59.33 fb	0.0056 %

Table 2: Numerical results for integrated cross sections for the charged-current Drell–Yan process mediated by a W boson in association with a hard jet at the LHC, with $\sqrt{s} = 7 \text{ TeV}$ and $\sqrt{s} = 14 \text{ TeV}$. Shown are the leading order results in picobarn (pb), the SQCD contributions in femtobarn (fb) and the relative corrections δ for the partonic subchannels and the inclusive result (incl.). Light quarks are implicitly summed over in the initial state, $q = u, d, c, s$. We consider $m_{\tilde{q}} = 600 \text{ GeV}$, $m_{\tilde{g}} = 500 \text{ GeV}$ and the cuts listed in Eq. (3.3) have been applied. Factorization and renormalization scale are set to $\mu = M_W$ (with MSTW 2008 NLO) .

c. m. energy of $\sqrt{s} = 7 \text{ TeV}$ and $\sqrt{s} = 14 \text{ TeV}$. Similar to the Z/γ^* +jet case, the SQCD corrections contribute between 0.004 – 0.006% to the individual channels and the inclusive result. The gluon-induced processes are slightly more affected than the quark-annihilation channels. The main cross section contribution comes from gluon-induced initial states, with increasing importance for higher c. m. energies. Thus the impact of the SQCD corrections on the inclusive cross section is somewhat enhanced at 14 TeV compared to 7 TeV.

3.5 W +jet kinematic distributions

The differential distributions for W +jet production at the LHC with $\sqrt{s} = 7 \text{ TeV}$ are shown in Figs. 7, 8, and 9. They correspond to distributions in transverse mass, lepton transverse momentum and rapidity, and jet transverse momentum and rapidity.

The transverse mass, $M_T(\ell\nu)$, and the $p_{T\ell}$ distributions are particularly relevant for the measurement of the W boson mass at hadron colliders. Here, the transverse mass is defined as $M_T(\ell\nu) = [(|p_{T,\ell}| + |\not{p}_T|)^2 - (\mathbf{p}_{T,\ell} + \mathbf{\not{p}}_T)^2]^{1/2}$.

Again, the results are very similar to those for Z/γ^* +jet production. The $M_T(\ell\nu)$ distributions, displayed in Figure 7, receive percent-level corrections due to SQCD effects, which are minimal and almost vanishing when the W boson is on-shell and maximal around squark and gluino thresholds in the high- $M_T(\ell\nu)$ region.

The relative corrections to the $p_{T,\ell}$ and $p_{T,\text{jet}}$ distributions, Figure 8 (left) and Figure 9 (left), peak around the average sparticle mass where they amount to about 1%, and grow negative in the high- p_T region, reaching a couple percent in the TeV region. The SQCD corrections in the lepton and jet rapidity distributions, Figure 8 (right) and Figure 9 (right), are flat and can safely be neglected in an experimental analysis.

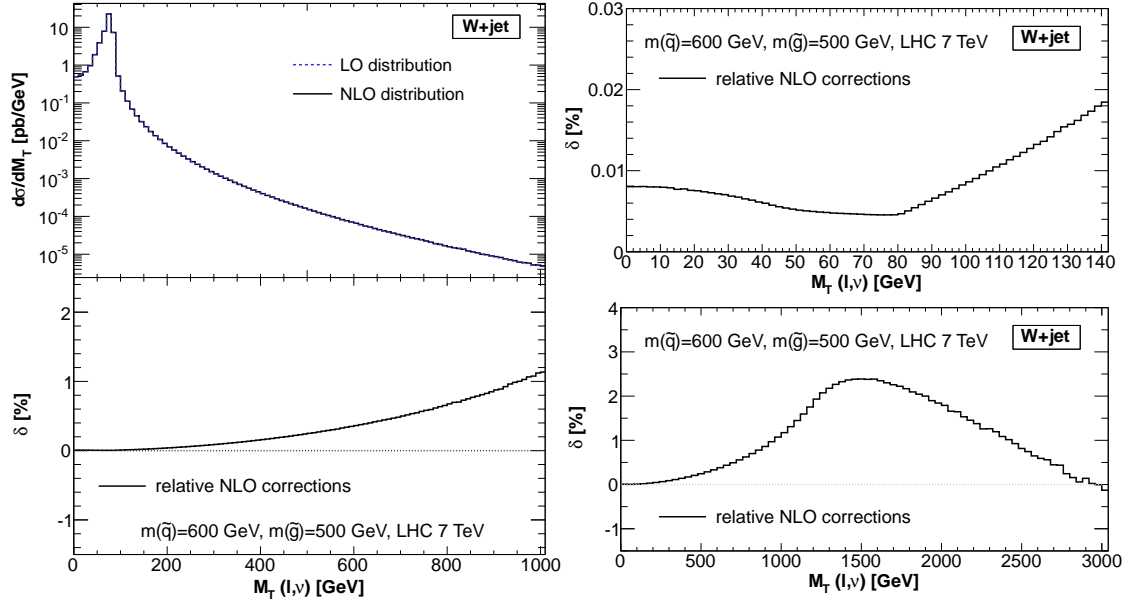


Figure 7: Differential distributions for the charged-current Drell–Yan process in association with a hard jet at the LHC. NLO SQCD corrections are calculated for $m_{\bar{q}} = 600$ GeV and $m_{\bar{g}} = 500$ GeV and the cuts given in Eq. (3.3) have been placed. Shown are the absolute differential distributions for the LO and NLO processes (top left) and the relative difference between NLO and LO distributions (bottom left) with respect to transverse mass $M_T(\ell\nu)$. In the right panels, the relative corrections around the W boson resonance and in the high- $M_T(\ell\nu)$ region are shown, respectively.

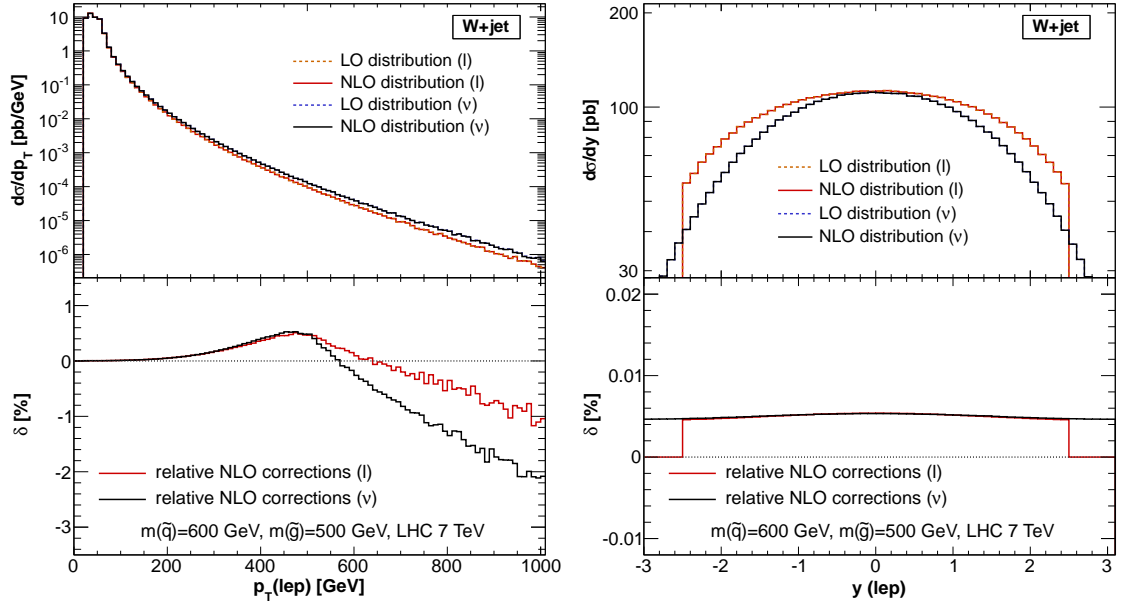


Figure 8: Lepton transverse momentum, $p_{T,\ell}$, (a) and lepton rapidity, y_ℓ , (b) distributions for the W +jet process at the LHC with $\sqrt{s} = 7$ TeV. The red line represents the charged lepton while the black line represents the neutrino (missing transverse momentum, \cancel{E}_T).

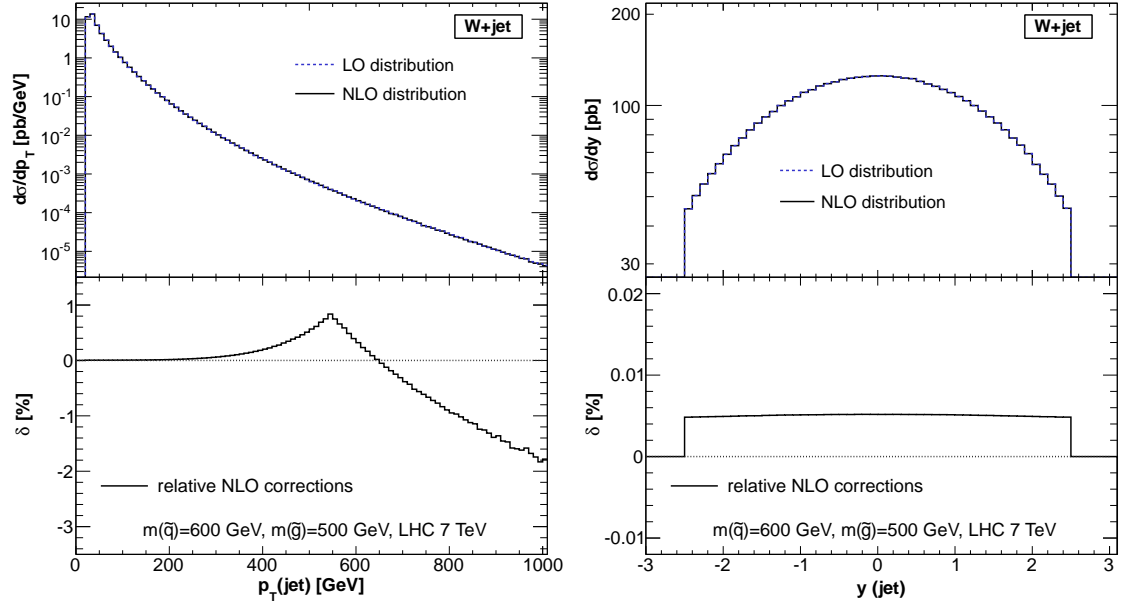


Figure 9: Jet transverse momentum, $p_{T,\text{jet}}$, (a) and jet rapidity, y_{jet} , (b) distributions for the $W+\text{jet}$ process at the LHC with $\sqrt{s} = 7$ TeV.

4. Conclusions

In this manuscript, we present a full treatment of the SQCD corrections to the neutral- and charged-current Drell–Yan process in association with a hard jet. We include the decay of the electroweak gauge bosons into a lepton pair or a lepton-neutrino pair, respectively, and take all off-shell effects due to the finite Z and W boson widths into account, as well as the contributions and interference effects of the photon-mediated diagrams in case of the neutral Drell–Yan process.

Even though the Drell–Yan process, with an associated jet, can not be used in any practical manner to set indirect limits on SUSY particle masses or SUSY parameters, it is important to study the impact of SUSY (and other BSM physics) contributions to SM processes. As standard candles, and important backgrounds to new physics at the LHC, it is necessary to understand the stability of EW gauge bosons production processes against BSM contributions.

We find that the relative corrections to the integrated cross section due to SQCD corrections are small, below the 0.5% level even for very light SUSY particles. Examining the differential distributions in conventional kinematic variables such as p_T , $M_{\ell\ell}$, or $M_T(\ell\nu)$, we find vanishing effects in the vicinity of the Z or W boson resonance peak, while the relative SQCD corrections can increase to 2 – 5% when the electroweak gauge bosons are far off-shell.

Acknowledgments

We are grateful to T. Hahn, S. Kallweit, and F. Petriello for useful discussions and helpful comments. This work was supported by the US DOE under contract No. DE-FG02-95ER40896.

A. Counterterms and renormalization constants

Here we list the counterterms for the renormalization of vertices and propagators in the SQCD one-loop amplitudes for Drell–Yan+jet production. All quarks are considered massless.

By using multiplicative renormalization, we replace in the QCD Lagrangian the left- and right-handed quark fields, $\Psi_{L,R}$, the gluon field, G^a , and the strong coupling constant, g_s , with

$$\Psi_{L,R} \rightarrow \sqrt{Z_{L,R}} \Psi_{L,R}, \quad G_\mu^a \rightarrow \sqrt{Z_G} G_\mu^a, \quad g_s \rightarrow Z_{g_s} g_s. \quad (\text{A.1})$$

Expanding $Z_i = 1 + \delta Z_i$, and introducing $\delta Z_{V,A} = \frac{1}{2}(\delta Z_L \pm \delta Z_R)$, we find the following Feynman rules for the self-energy and vertex counterterms that are relevant in our calculation.

$$\begin{array}{c} \overline{p}_\gamma \\ | \\ q \end{array} \text{---} \times \text{---} q : i\not{p}(\delta Z_V - \delta Z_A \gamma_5), \quad (\text{A.2})$$

$$\text{Feynman diagram: a wavy line labeled } \gamma, \mu \text{ enters a vertex from the left. From this vertex, two straight lines branch out to the right, both labeled } q. \text{ The diagram is followed by the expression } : -iee_q \gamma^\mu (\delta Z_V - \delta Z_A \gamma_5), \text{ and then (A.3).}$$

$$\begin{array}{c} \text{---}\gamma\text{---} \\ | \\ Z, \mu \end{array} \times \begin{array}{l} \nearrow q \\ \searrow q \end{array} : -\frac{ie}{c_W s_W} \gamma^\mu (g_V^q - g_A^q \gamma_5) (\delta Z_V - \delta Z_A \gamma_5), \quad \begin{aligned} g_V^q &= \frac{1}{2} I_3^q - e_q s_W^2, \\ g_A^q &= \frac{1}{2} I_3^q, \end{aligned} \quad (\text{A.4})$$

$$\begin{array}{c} \diagup \\ \text{---} \times \text{---} \\ \diagdown \end{array} \begin{array}{c} q' \\ q \end{array} : -\frac{ie}{2\sqrt{2}s_W} V_{qq'}^{\text{CKM}} \gamma^\mu (1 - \gamma_5) (\delta Z_V + \delta Z_A), \quad (\text{A.5})$$

$$\begin{array}{c} \text{wavy line} \\ g, a, \mu \end{array} \times \begin{array}{c} \nearrow q \\ \searrow q \end{array} : -ig_s T^a \gamma^\mu (\delta Z_V - \delta Z_A \gamma_5 + \delta Z_{g_s} + \frac{1}{2} \delta Z_G), \quad (\text{A.6})$$

where e_q is the electric charge of quark q and I_3^q denotes the eigenvalue of the third component of its weak isospin. T^a , $a = 1..8$, are the color matrices of $SU(3)_C$, while we have omitted the color indices of the quarks. We use the abbreviation s_W and c_W for the sine and cosine of the electroweak mixing angle θ_W . As usual, q and q' are quarks of opposite isospin and $V_{qq'}^{\text{CKM}}$ is the corresponding entry of the CKM quark mixing matrix.

For the renormalization of the gluon field and the strong coupling we use the \overline{MS} scheme, modified to decouple the squarks and the gluino [53, 54]. The renormalization

constant of the strong coupling is then given by, see also [52],

$$\delta Z_{g_s} = -\frac{\alpha_s}{4\pi} \left\{ \frac{\beta_0}{2} \Delta + \frac{1}{12} \sum_{\tilde{q}} \log \left(\frac{m_{\tilde{q}}^2}{\mu^2} \right) + \log \left(\frac{m_{\tilde{g}}^2}{\mu^2} \right) \right\}, \quad (\text{A.7})$$

where the sum runs over the twelve squark eigenstates, μ is the renormalization scale, $\Delta = 1/\epsilon - \gamma_E + \ln 4\pi$; and

$$\beta_0 = -\frac{2}{3}N - \frac{1}{3}n_{\tilde{q}}, \quad (\text{A.8})$$

with $N = 3$ and $n_{\tilde{q}} = 6$ for the six squark flavors, includes only the gluino and squark contributions. In this case, there is a simple relation between the gluon field and strong coupling renormalization constants,

$$\delta Z_G = -2 \delta Z_{g_s}, \quad (\text{A.9})$$

and they actually cancel out in Eq. (A.6) and do not enter our calculation.

In the quark sector, we use the on-shell scheme to fix the renormalization constants $\delta Z_{V,A}$ of the (massless) quarks, i.e. the renormalization constants are obtained by evaluating the vector and axial components of the quark self-energy at the on-shell quark mass,

$$\delta Z_{V,A} = -\Sigma_{V,A}(p^2 = 0). \quad (\text{A.10})$$

The SQCD corrections to the quark self-energy consist of a squark-gluino bubble insertion in the quark line and can be expressed in the following general, compact form [52],

$$\begin{aligned} \Sigma_V(p^2) &= -\frac{\alpha_s}{4\pi} \sum_i \left((g_S^i)^2 + (g_P^i)^2 \right) \frac{2}{3} B_1(p^2, m_{\tilde{g}}, m_{\tilde{q}_i}), \\ \Sigma_A(p^2) &= \frac{\alpha_s}{4\pi} \sum_i 2g_S^i g_P^i \frac{2}{3} B_1(p^2, m_{\tilde{g}}, m_{\tilde{q}_i}). \end{aligned} \quad (\text{A.11})$$

Here, $B_1(p^2, m_1^2, m_2^2)$ is the two-point function as defined in [56]. i sums over the two squark mass eigenstates and g_S^i and g_P^i are scalar and pseudoscalar couplings. In the limit of no left-right mixing in the squark sector, $g_S^{L,R} = \pm 1$ and $g_P^{L,R} = 0$. When considering the mixing, then

$$\begin{aligned} g_S^{1,2} &= \cos \theta_{\tilde{q}} g_S^{L,R} \pm \sin \theta_{\tilde{q}} g_S^{R,L}, \\ g_P^{1,2} &= \cos \theta_{\tilde{q}} g_P^{L,R} \pm \sin \theta_{\tilde{q}} g_P^{R,L}, \end{aligned} \quad (\text{A.12})$$

where $\theta_{\tilde{q}}$ is the squark mixing angle (notation as in [52]).

In our numerical study, we neglect the left-right squark mixing, and consider degenerate squark masses, $m_{\tilde{q}_1} = m_{\tilde{q}_2} = m_{\tilde{q}}$. In this limit, we find $\Sigma_A(p^2) = 0$ and the only renormalization constant that remains is δZ_V , with

$$\delta Z_V = -\frac{\alpha_s}{3\pi} \left\{ \Delta + \frac{3m_{\tilde{g}}^2 - m_{\tilde{q}}^2}{2(m_{\tilde{g}}^2 - m_{\tilde{q}}^2)} - \frac{m_{\tilde{g}}^4}{(m_{\tilde{g}}^2 - m_{\tilde{q}}^2)^2} \ln \left(\frac{m_{\tilde{g}}^2}{\mu_R^2} \right) + \frac{m_{\tilde{q}}^2(2m_{\tilde{g}}^2 - m_{\tilde{q}}^2)}{(m_{\tilde{g}}^2 - m_{\tilde{q}}^2)^2} \ln \left(\frac{m_{\tilde{q}}^2}{\mu_R^2} \right) \right\}. \quad (\text{A.13})$$

References

- [1] CMS, *Measurement of the Drell-Yan Cross Section in pp Collisions at $\sqrt{s} = 7$ TeV*, [arXiv:1108.0566](#).
- [2] CMS Collaboration, *Measurement of the Inclusive W and Z Production Cross Sections in pp Collisions at $\sqrt{s} = 7$ TeV*, [arXiv:1107.4789](#).
- [3] ATLAS Collaboration, *Measurement of the transverse momentum distribution of Z/gamma* bosons in proton-proton collisions at $\sqrt{s}=7$ TeV with the ATLAS detector*, [arXiv:1107.2381](#).
- [4] ATLAS Collaboration, G. Aad *et. al.*, *Measurement of the $W \rightarrow l\nu$ and Z/gamma* $\rightarrow ll$ production cross sections in proton-proton collisions at $\sqrt{s} = 7$ TeV with the ATLAS detector*, *JHEP* **1012** (2010) 060, [[arXiv:1010.2130](#)].
- [5] R. D. Ball, L. Del Debbio, S. Forte, A. Guffanti, J. I. Latorre, *et. al.*, *A first unbiased global NLO determination of parton distributions and their uncertainties*, *Nucl.Phys.* **B838** (2010) 136–206, [[arXiv:1002.4407](#)].
- [6] R. Thorne, A. Martin, W. Stirling, and G. Watt, *The Effects of combined HERA and recent Tevatron $W \rightarrow l \nu$ charge asymmetry data on the MSTW PDFs*, *PoS DIS2010* (2010) 052, [[arXiv:1006.2753](#)].
- [7] H.-L. Lai, M. Guzzi, J. Huston, Z. Li, P. M. Nadolsky, *et. al.*, *New parton distributions for collider physics*, *Phys.Rev.* **D82** (2010) 074024, [[arXiv:1007.2241](#)].
- [8] M. Dittmar, F. Pauss, and D. Zurcher, *Towards a precise parton luminosity determination at the CERN LHC*, *Phys.Rev.* **D56** (1997) 7284–7290, [[hep-ex/9705004](#)].
- [9] T. G. Rizzo, *Z' phenomenology and the LHC*, [hep-ph/0610104](#).
- [10] C.-W. Chiang, N. D. Christensen, G.-J. Ding, and T. Han, *Discovery in Drell-Yan Processes at the LHC*, [arXiv:1107.5830](#).
- [11] ATLAS Collaboration, *Detector and physics performance technical design report. Volume 2*, [ATLAS-TDR-15](#).
- [12] CMS Collaboration, G. Bayatian *et. al.*, *CMS technical design report, volume II: Physics performance*, *J.Phys.G* **G34** (2007) 995–1579.
- [13] G. Dissertori, *Prospects for measuring hard processes the LHC*, . Talk presented at the HP² Workshop, Zurich, Switzerland (2006).
- [14] R. Hamberg, W. van Neerven, and T. Matsuura, *A Complete calculation of the order α_s^2 correction to the Drell-Yan K factor*, *Nucl.Phys.* **B359** (1991) 343–405.
- [15] R. V. Harlander and W. B. Kilgore, *Next-to-next-to-leading order Higgs production at hadron colliders*, *Phys.Rev.Lett.* **88** (2002) 201801, [[hep-ph/0201206](#)].
- [16] C. Anastasiou, L. J. Dixon, K. Melnikov, and F. Petriello, *Dilepton rapidity distribution in the Drell-Yan process at NNLO in QCD*, *Phys.Rev.Lett.* **91** (2003) 182002, [[hep-ph/0306192](#)].
- [17] C. Anastasiou, L. J. Dixon, K. Melnikov, and F. Petriello, *High precision QCD at hadron colliders: Electroweak gauge boson rapidity distributions at NNLO*, *Phys.Rev.* **D69** (2004) 094008, [[hep-ph/0312266](#)].

- [18] K. Melnikov and F. Petriello, *The W boson production cross section at the LHC through $\mathcal{O}(\alpha_s^2)$* , Phys.Rev.Lett. **96** (2006) 231803, [[hep-ph/0603182](#)].
- [19] K. Melnikov and F. Petriello, *Electroweak gauge boson production at hadron colliders through $\mathcal{O}(\alpha_s^2)$* , Phys.Rev. **D74** (2006) 114017, [[hep-ph/0609070](#)].
- [20] S. Catani, L. Cieri, G. Ferrera, D. de Florian, and M. Grazzini, *Vector boson production at hadron colliders: A Fully exclusive QCD calculation at NNLO*, PRLTA,103,082001.2009 **103** (2009) 082001, [[arXiv:0903.2120](#)].
- [21] S. Catani, G. Ferrera, and M. Grazzini, *W boson production at hadron colliders: the lepton charge asymmetry in NNLO QCD*, JHEP **1005** (2010) 006, [[arXiv:1002.3115](#)].
- [22] S. Alioli, P. Nason, C. Oleari, and E. Re, *Vector boson plus one jet production in POWHEG*, JHEP **1101** (2011) 095, [[arXiv:1009.5594](#)].
- [23] S. Frixione, P. Nason, and C. Oleari, *Matching NLO QCD computations with Parton Shower simulations: the POWHEG method*, JHEP **0711** (2007) 070, [[arXiv:0709.2092](#)].
- [24] K. Hamilton, P. Richardson, and J. Tully, *A Positive-Weight Next-to-Leading Order Monte Carlo Simulation of Drell-Yan Vector Boson Production*, JHEP **0810** (2008) 015, [[arXiv:0806.0290](#)].
- [25] S. Frixione and B. R. Webber, *The MC@NLO 3.3 Event Generator*, [hep-ph/0612272](#).
- [26] U. Baur, S. Keller, and W. Sakumoto, *QED radiative corrections to Z boson production and the forward backward asymmetry at hadron colliders*, Phys.Rev. **D57** (1998) 199–215, [[hep-ph/9707301](#)].
- [27] U. Baur, S. Keller, and D. Wackerth, *Electroweak radiative corrections to W boson production in hadronic collisions*, Phys.Rev. **D59** (1999) 013002, [[hep-ph/9807417](#)].
- [28] U. Baur, O. Brein, W. Hollik, C. Schappacher, and D. Wackerth, *Electroweak radiative corrections to neutral current Drell-Yan processes at hadron colliders*, Phys.Rev. **D65** (2002) 033007, [[hep-ph/0108274](#)].
- [29] S. Dittmaier and M. Krämer, *Electroweak radiative corrections to W boson production at hadron colliders*, Phys.Rev. **D65** (2002) 073007, [[hep-ph/0109062](#)].
- [30] S. Dittmaier and M. Huber, *Radiative corrections to the neutral-current Drell-Yan process in the Standard Model and its minimal supersymmetric extension*, JHEP **1001** (2010) 060, [[arXiv:0911.2329](#)].
- [31] S. Brensing, S. Dittmaier, M. Krämer, and A. Mück, *Radiative corrections to W^- boson hadroproduction: Higher-order electroweak and supersymmetric effects*, Phys.Rev. **D77** (2008) 073006, [[arXiv:0710.3309](#)].
- [32] P. Richardson, R. Sadykov, A. Saponov, M. Seymour, and P. Skands, *QCD parton showers and NLO EW corrections to Drell-Yan*, [arXiv:1011.5444](#).
- [33] V. Zykunov, *Total calculation of electroweak corrections to the Drell-Yan process for LHC*, Phys.Atom.Nucl. **71** (2008) 732–745.
- [34] G. Balossini, G. Montagna, C. Carloni Calame, M. Moretti, M. Treccani, et. al., *Electroweak and QCD corrections to Drell Yan processes*, Acta Phys.Polon. **B39** (2008) 1675, [[arXiv:0805.1129](#)]. In honour of the 60th birthday of Prof. S. Jadach.

- [35] G. Balossini, C. Carloni Calame, G. Montagna, M. Moretti, O. Nicrosini, *et. al.*, *Combining electroweak and QCD corrections to Drell-Yan processes at hadron colliders*, AIP Conf.Proc. **1317** (2011) 25–32.
- [36] W. B. Kilgore and C. Sturm, *Two-Loop Virtual Corrections to Drell-Yan Production at order $\alpha_s\alpha^3$* , [[arXiv:1107.4798](#)].
- [37] W. Giele, E. Glover, and D. A. Kosower, *Higher order corrections to jet cross-sections in hadron colliders*, Nucl.Phys. **B403** (1993) 633–670, [[hep-ph/9302225](#)].
- [38] J. van der Bij and E. Glover, *Z Boson production and decay via gluons*, Nucl.Phys. **B313** (1989) 237.
- [39] J. M. Campbell and R. Ellis, *Next-to-leading order corrections to W+2 jet and Z+2 jet production at hadron colliders*, Phys.Rev. **D65** (2002) 113007, [[hep-ph/0202176](#)].
- [40] W. Hollik, T. Kasprzik, and B. Kniehl, *Electroweak corrections to W-boson hadroproduction at finite transverse momentum*, Nucl.Phys. **B790** (2008) 138–159, [[arXiv:0707.2553](#)].
- [41] J. H. Kühn, A. Kulesza, S. Pozzorini, and M. Schulze, *Electroweak corrections to hadronic production of W bosons at large transverse momenta*, Nucl.Phys. **B797** (2008) 27–77, [[arXiv:0708.0476](#)].
- [42] J. H. Kühn, A. Kulesza, S. Pozzorini, and M. Schulze, *Logarithmic electroweak corrections to hadronic Z+1 jet production at large transverse momentum*, Phys.Lett. **B609** (2005) 277–285, [[hep-ph/0408308](#)].
- [43] J. H. Kühn, A. Kulesza, S. Pozzorini, and M. Schulze, *One-loop weak corrections to hadronic production of Z bosons at large transverse momenta*, Nucl.Phys. **B727** (2005) 368–394, [[hep-ph/0507178](#)].
- [44] J. H. Kühn, A. Kulesza, S. Pozzorini, and M. Schulze, *Electroweak corrections to large transverse momentum production of W bosons at the LHC*, Phys.Lett. **B651** (2007) 160–165, [[hep-ph/0703283](#)].
- [45] A. Denner, S. Dittmaier, T. Kasprzik, and A. Mück, *Electroweak corrections to W + jet hadroproduction including leptonic W-boson decays*, JHEP **0908** (2009) 075, [[arXiv:0906.1656](#)].
- [46] A. Denner, S. Dittmaier, T. Kasprzik, and A. Mück, *Electroweak corrections to dilepton + jet production at hadron colliders*, JHEP **1106** (2011) 069, [[arXiv:1103.0914](#)].
- [47] R. Ellis, W. Giele, Z. Kunszt, K. Melnikov, and G. Zanderighi, *One-loop amplitudes for W+3 jet production in hadron collisions*, JHEP **0901** (2009) 012, [[arXiv:0810.2762](#)].
- [48] C. Berger, Z. Bern, L. J. Dixon, F. Febres Cordero, D. Forde, *et. al.*, *Next-to-Leading Order QCD Predictions for W+3-Jet Distributions at Hadron Colliders*, Phys.Rev. **D80** (2009) 074036, [[arXiv:0907.1984](#)].
- [49] C. Berger, Z. Bern, L. J. Dixon, F. Febres Cordero, D. Forde, *et. al.*, *Next-to-Leading Order QCD Predictions for Z,gamma+3-Jet Distributions at the Tevatron*, Phys.Rev. **D82** (2010) 074002, [[arXiv:1004.1659](#)].
- [50] C. Berger, Z. Bern, L. J. Dixon, F. Febres Cordero, D. Forde, *et. al.*, *Precise Predictions for W + 4 Jet Production at the Large Hadron Collider*, Phys.Rev.Lett. **106** (2011) 092001, [[arXiv:1009.2338](#)].

- [51] G. Gounaris, J. Layssac, and F. M. Renard, *Remarkable virtual SUSY effects in W^{+-} production at high energy hadron colliders*, Phys.Rev. **D77** (2008) 013003, [[arXiv:0709.1789](#)].
- [52] S. Berge, W. Hollik, W. M. Möhle, and D. Wackeroth, *SUSY QCD one-loop effects in (un)polarized top-pair production at hadron colliders*, Phys.Rev. **D76** (2007) 034016, [[hep-ph/0703016](#)].
- [53] J. C. Collins, F. Wilczek, and A. Zee, *Low-Energy Manifestations of Heavy Particles: Application to the Neutral Current*, Phys.Rev. **D18** (1978) 242.
- [54] P. Nason, S. Dawson, and R. Ellis, *The One Particle Inclusive Differential Cross-Section for Heavy Quark Production in Hadronic Collisions*, Nucl.Phys. **B327** (1989) 49–92.
- [55] T. Hahn, *Generating Feynman diagrams and amplitudes with FeynArts 3*, Comput.Phys.Comm. **140** (2001) 418–431, [[hep-ph/0012260](#)].
- [56] T. Hahn and M. Perez-Victoria, *Automatized one loop calculations in four-dimensions and D-dimensions*, Comput.Phys.Comm. **118** (1999) 153–165, [[hep-ph/9807565](#)].
- [57] P. Nogueira, *Automatic Feynman graph generation*, J.Comput.Phys. **105** (1993) 279–289.
- [58] J. Vermaseren, *New features of FORM*, [math-ph/0010025](#).
- [59] C. Anastasiou and A. Lazopoulos, *Automatic integral reduction for higher order perturbative calculations*, JHEP **0407** (2004) 046, [[hep-ph/0404258](#)].
- [60] T. Hahn, *CUBA: A Library for multidimensional numerical integration*, Comput.Phys.Comm. **168** (2005) 78–95, [[hep-ph/0404043](#)].
- [61] R. Ellis and G. Zanderighi, *Scalar one-loop integrals for QCD*, JHEP **0802** (2008) 002, [[arXiv:0712.1851](#)].
- [62] F. Jegerlehner, *Facts of life with $\gamma(5)$* , Eur.Phys.J. **C18** (2001) 673–679, [[hep-th/0005255](#)].
- [63] M. S. Chanowitz, M. Furman, and I. Hinchliffe, *The Axial Current in Dimensional Regularization*, Nucl.Phys. **B159** (1979) 225.
- [64] S. Larin, *The Renormalization of the axial anomaly in dimensional regularization*, Phys.Lett. **B303** (1993) 113–118, [[hep-ph/9302240](#)].
- [65] **Particle Data Group** Collaboration, K. Nakamura *et. al.*, *Review of particle physics*, J.Phys. **G37** (2010) 075021.
- [66] A. Martin, W. Stirling, R. Thorne, and G. Watt, *Parton distributions for the LHC*, Eur.Phys.J. **C63** (2009) 189–285, [[arXiv:0901.0002](#)].
- [67] M. R. Whalley, D. Bourilkov, and R. C. Group, *The Les Houches Accord PDFs (LHAPDF) and Lhaglu*, [hep-ph/0508110](#).
- [68] **CMS** Collaboration, S. Chatrchyan *et. al.*, *Search for New Physics with Jets and Missing Transverse Momentum in pp collisions at $\sqrt{s} = 7$ TeV*, [arXiv:1106.4503](#).
- [69] **ATLAS** Collaboration, G. Aad *et. al.*, *Search for supersymmetric particles in events with lepton pairs and large missing transverse momentum in $\sqrt{s} = 7$ TeV proton-proton collisions with the ATLAS experiment*, [arXiv:1103.6214](#).